Plane-Wave Diffraction by a Slit Formed by Two Semi-Infinite Parallel-Plate Waveguides—Part II: The Case of *E* Polarization

Takashi Nagasaka, Ryota Mimura, and Kazuya Kobayashi

Abstract − The diffraction by a slit formed by two semi-infinite parallel-plate waveguides is rigorously analyzed using the Wiener−Hopf technique for the *E*-polarized plane-wave incidence. Applying a method similar to that developed in Part I of this two-part article, exact and high-frequency asymptotic solutions are both obtained. Numerical examples of the far-field intensity are presented, and scattering characteristics of the waveguide slit are discussed. Some comparisons with our results for *H* polarization are also given.

1. Introduction

The analysis of electromagnetic scattering by slits formed by parallel-plate waveguides (i.e., tandem slits) is important in electromagnetic theory, as well as microwave and optical instrumentation. There are several important articles analyzing diffraction problems related to tandem slits [1−5]. Among these, [3] is most relevant to this two-part article and analyzed the plane-wave diffraction by a perfectly conducting tandem slit, with the aid of the Wiener−Hopf technique, leading to a high-frequency asymptotic solution.

In Part I of this two-part article [6], we considered the same waveguide slit geometry as in [3] and rigorously analyzed the *H*-polarized plane wave diffraction using the Wiener−Hopf technique. As a result, we successfully have obtained a novel high-frequency solution to the waveguide slit problem in the form of a complete asymptotic series by using rigorous asymptotics [7, 8] developed by the authors for the analysis of modified Wiener−Hopf geometries. Note that our asymptotic solution incorporates all the higher order diffraction effects; hence, it is valid, even for slit width comparable to the incident wavelength.

This article serves as the second part of this two-part article, and we analyze the *E*-polarized plane wave diffraction by the same, waveguide slit geometry as considered in Part I. The method of solution is based on the Wiener−Hopf technique, and we apply a method similar to that developed for the analysis of *H* polarization. The Wiener−Hopf analysis leads first to an exact (formal) solution and then to a high-frequency asymptotic solution. As has been previously emphasized, the latter solution contains all the higher order diffraction terms and, hence, serves as a strong solution. The scattered field is subsequently evaluated, resulting in transverse electric modes inside the waveguides and a far-field expression outside the waveguides. Numerical examples are presented for various physical parameters, and the scattering characteristics of the waveguide slit are discussed. Some comparisons with the results for *H* polarization [6] are given. The time factor is assumed to be $\exp(-i\omega t)$ and suppressed throughout the article.

Manuscript received 31 December 2022.

Takashi Nagasaka, Ryota Mimura, and Kazuya Kobayashi are with the Department of Electrical, Electronic, and Communication Engineering, Chuo University, 1-13-27 Kasuga, Bunkyo-ku, Tokyo 112-8551, Japan; e-mail: nagasaka@elect.chuo-u.ac.jp, a17.g664@g.chuo-u.ac.jp, kazuya@tamacc.chuo-u.ac.jp.

2. Formulation of the Problem

The geometry of the waveguide slit is shown in Figure 1, where the plates of the waveguides are infinitely thin and uniform in the y direction, and ϕ^i denotes the *E*-polarized plane wave. Let the total electric field $\phi^t(x,z)[\equiv E_y^t(x,z)]$ be defined by

$$\begin{aligned}\phi^t(x,z) &= \phi^i(x,z) + \phi(x,z) + R\phi^r(x,z), \quad x > b \\ &= \phi(x,z), \quad |x| < b \\ &= \phi(x,z), \quad x < -b \end{aligned} \tag{1}$$

where $\phi^i(x,z)$ is the incident field defined by

$$\phi^i(x,z) = e^{-ik(x\sin\theta_0 + z\cos\theta_0)}, \quad 0 < \theta_0 < \pi/2 \tag{2}$$

with $k[=\omega(\varepsilon_0\mu_0)^{1/2}]$ being the free-space wavenumber. In (1), $R\phi^r(x,z)$ denotes the reflected field, where

$$\phi^r(x,z) = e^{ik(x\sin\theta_0 - z\cos\theta_0)} \tag{3}$$

and $R = -e^{-2ikb\sin\theta_0}$ is the reflection coefficient. In the following analysis, we assume that the medium is slightly lossy as in $k = k_1 + ik_2$, $0 < k_1 \ll k_2$.

We define the Fourier transform of $\phi(x,z)$ with respect to z as

$$\Phi(x,\alpha) = (2\pi)^{-1/2}\int_{-\infty}^{\infty}\phi(x,z)e^{i\alpha z}dz, \quad \alpha = \sigma + i\tau \tag{4}$$

We also define the Fourier integrals as

$$\Phi_\pm(x,\alpha) = \pm(2\pi)^{-1/2}\int_{\pm a}^{\pm\infty}\phi(x,z)e^{i\alpha(z\mp a)}dz \tag{5}$$

$$\Phi_1(x,\alpha) = (2\pi)^{-1/2}\int_{-a}^{a}\phi(x,z)e^{i\alpha z}dz \tag{6}$$

In view of the radiation condition, we can verify that $\Phi(x,\alpha)$ and $\Phi_\pm(x,\alpha)$ are regular in $|\tau| < k_2\cos\theta_0$

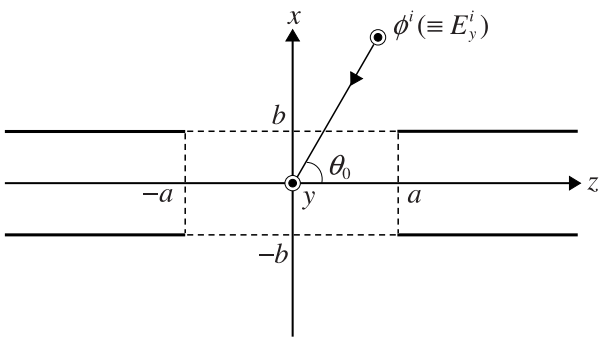

Figure 1. Geometry of the problem.

and $\tau \gtrless \mp k_2 \cos\theta_0$, respectively, whereas $\Phi_1(x,\alpha)$ is an entire function.

In view of the boundary conditions for tangential electromagnetic fields, we see that

$$E_y^t(\pm b, z) = 0, \quad |z| > a \tag{7}$$

$$E_y^t(\pm b + 0, z) = E_y^t(\pm b - 0, z), \quad |z| < a \tag{8}$$

$$H_z^t(\pm b + 0, z) = H_z^t(\pm b - 0, z), \quad |z| < a \tag{9}$$

where the superscript t implies the total field. The tangential component of the total electric field is continuous across $x = \pm b$ for $-\infty < z < \infty$. In contrast, the tangential component of the total magnetic field is continuous across $x = \pm b$ only for $|z| < a$.

Taking the Fourier transform of the two-dimensional Helmholtz equation and solving the resulting transformed wave equations, we derive that

$$\begin{aligned}\Phi(x,\alpha) &= A(\alpha)e^{-\gamma(x-b)}, \quad x > b \\ &= A(\alpha)\sinh[\gamma(x+b)]/\sinh(2\gamma b) \\ &\quad -B(\alpha)\sinh[\gamma(x-b)]/\sinh(2\gamma b), \quad |x| < b \\ &= B(\alpha)e^{\gamma(x+b)}, \quad x < -b\end{aligned} \tag{10}$$

where $\gamma = (\alpha^2 - k^2)^{1/2}$ with $\mathrm{Re}\gamma > 0$, and $A(\alpha)$ and $B(\alpha)$ are unknown spectral functions.

Given the boundary conditions in the Fourier transform domain, we obtain that

$$A(\alpha) + B(\alpha) = S_1(\alpha) \tag{11}$$

$$A(\alpha) - B(\alpha) = D_1(\alpha) \tag{12}$$

$$\begin{aligned}&e^{-i\alpha a}J_-(b,\alpha) + e^{i\alpha a}J_+(b,\alpha) \\ &\quad - \left(A_1 e^{i\alpha a} - A_2 e^{-i\alpha a}\right)/(\alpha - k\cos\theta_0) \\ &\quad = -\gamma A(\alpha)[\cos(2\gamma b)/\sin(2\gamma b) + 1] \\ &\quad + \gamma B(\alpha)/\sin(2\gamma b)\end{aligned} \tag{13}$$

$$\begin{aligned}&e^{-i\alpha a}J_-(-b,\alpha) + e^{i\alpha a}J_+(-b,\alpha) \\ &\quad = \gamma A(\alpha)/\sin(2\gamma b) \\ &\quad - \gamma B(\alpha)[\cos(2\gamma b)/\sin(2\gamma b) + 1]\end{aligned} \tag{14}$$

where

$$S_1(\alpha) = \Phi_1(b,\alpha) + \Phi_1(-b,\alpha) \tag{15}$$

$$D_1(\alpha) = \Phi_1(b,\alpha) - \Phi_1(-b,\alpha) \tag{16}$$

$$J_\pm(\pm b, \alpha) = \Phi'_\pm(\pm b + 0, \alpha) - \Phi'_\pm(\pm b - 0, \alpha) \tag{17}$$

$$A_{1,2} = -2k\sin\theta_0 e^{-ikb\sin\theta_0} e^{\mp ika\cos\theta_0}/(2\pi)^{1/2} \tag{18}$$

In (17), the prime denotes differentiation with respect to x.

Carrying out some manipulations with the aid of boundary conditions, we arrive at

$$-S_1(\alpha)/L(\alpha) = e^{i\alpha a}U_{(+)}(\alpha) + e^{-i\alpha a}U_-(\alpha) \tag{19}$$

$$-D_1(\alpha)/N(\alpha) = e^{i\alpha a}V_{(+)}(\alpha) + e^{-i\alpha a}V_-(\alpha) \tag{20}$$

where

$$\left.\begin{matrix}U_{(+)}(\alpha) \\ U_-(\alpha)\end{matrix}\right\} = J_\pm^s(\alpha) \mp A_{1,2}/(\alpha - k\cos\theta_0) \tag{21}$$

$$\left.\begin{matrix}V_{(+)}(\alpha) \\ V_-(\alpha)\end{matrix}\right\} = J_\pm^d(\alpha) \mp A_{1,2}/(\alpha - k\cos\theta_0) \tag{22}$$

$$L(\alpha) = e^{-\gamma b}\cosh(\gamma b)/\gamma \tag{23}$$

$$N(\alpha) = e^{-\gamma b}\sinh(\gamma b)/\gamma \tag{24}$$

with

$$J_\pm^s(\alpha) = J_\pm(b,\alpha) + J_\pm(-b,\alpha) \tag{25}$$

$$J_\pm^d(\alpha) = J_\pm(b,\alpha) - J_\pm(-b,\alpha) \tag{26}$$

In the previously mentioned notations, the subscripts $+$ and $-$ imply that the functions are regular in the upper $(\tau > -k_2\cos\theta_0)$ and the lower $(\tau < k_2\cos\theta_0)$ half plane, respectively, whereas the subscript $(+)$ implies that the functions are regular in $\tau > -k_2\cos\theta_0$, except for a simple pole at $\alpha = k\cos\theta_0$. Thus, (19) and (20) are the desired simultaneous Wiener–Hopf equations.

3. Solution of the Wiener–Hopf Equations

The kernel function defined by (23) and (24) cane be factorized as in [9]

$$L(\alpha) = L_+(\alpha)L_-(\alpha) \tag{27}$$

$$N(\alpha) = N_+(\alpha)N_-(\alpha) \tag{28}$$

where $L_\pm(\alpha)$ and $N_\pm(\alpha)$ are split functions defined by

$$\begin{aligned} L_\pm(\alpha) &= [\cos(kb)]^{1/2} e^{i\pi/4}(k \pm \alpha)^{-1/2} \\ &\cdot \exp(\pm(i\alpha b/\pi)\{1 - C + \ln[\pi/(2kb)] + i\pi/2\}) \\ &\cdot \exp\{(i\gamma b/\pi)\ln[(\pm\alpha - \gamma)/k]\} \\ &\cdot \prod_{\substack{n=1 \\ \text{odd}}}^{\infty} [1 \pm \alpha/(i\gamma_n)] e^{\pm 2i\alpha b/(n\pi)} \end{aligned} \tag{29}$$

$$\begin{aligned} N_\pm(\alpha) &= [\sin(kb)/k]^{1/2} \\ &\cdot \exp(\pm(i\alpha b/\pi)\{1 - C + \ln[2\pi/(kb)] + i\pi/2\}) \\ &\cdot \exp\{(i\gamma b/\pi)\ln[(\pm\alpha - \gamma)/k]\} \\ &\cdot \prod_{\substack{n=2 \\ \text{even}}}^{\infty} [1 \pm \alpha/(i\gamma_n)] e^{\pm 2i\alpha b/(n\pi)} \end{aligned} \tag{30}$$

with $C = 0.57721566$ being the Euler constant, where

$$\begin{aligned} \gamma_n &= -ik, \quad n = 0, \\ &= \left\{[n\pi/(2b)]^2 - k^2\right\}^{1/2}, \quad n \geq 1 \end{aligned} \tag{31}$$

Carrying out the factorization and decomposition procedures for (19) and making some arrangements, we arrive at

$$\begin{aligned} U^{s,d}_{(+)}(\alpha) = \Bigg[&-\frac{A_1 L_+(k\cos\theta_0)}{\alpha - k\cos\theta_0} \mp \frac{A_2 L_-(k\cos\theta_0)}{\alpha + k\cos\theta_0} \\ &\pm \frac{1}{\pi i}\int_k^{k+i\infty} \frac{F_+(\beta)U^{s,d}_{(+)}(\beta)}{(\beta - k)^{1/2}(\beta + \alpha)} e^{2i\beta a} d\beta \Bigg] \Big/ L_+(\alpha) \end{aligned} \tag{32}$$

where

$$F_+(\beta) = \cosh^2(\gamma b)/\left[L_+(\beta)(\beta + k)^{1/2}\right] \tag{33}$$

Therefore, (32) provides an exact solution of (19), but it is formal because it involves infinite branch-cut integrals with unknown integrals. We need to derive explicit approximate expressions of (32) for the solution to be complete.

By using the method of asymptotic solutions developed by [7, 8] and making some manipulations, as was done in Part I [6], we finally obtain that

$$\begin{aligned} \left.\begin{matrix} U_{(+)}(\alpha) \\ U_-(\alpha) \end{matrix}\right\} \sim \Bigg\{ &\mp \frac{A_{1,2} L_\pm(k\cos\theta_0)}{\alpha - k\cos\theta_0} + A_{2,1}\eta_{f1,f2}(\pm\alpha) \\ &+ \sum_{n=0}^{\infty} \left[\xi^f_{0n}(\pm\alpha)\left(f^{us} \mp f^{ud}_n\right)/2\right] \Bigg\} \Big/ L_\pm(\alpha) \end{aligned} \tag{34}$$

where

$$f^{us,ud}_n = \frac{1}{n!}\frac{d^n}{d\beta^n}\left[J^s_+(\beta) \pm J^s_-(-\beta)\right]\Big|_{\beta=k} \tag{35}$$

$$\eta_{f1,f2}(\alpha) = \frac{\xi^f_{00}(\alpha) - \xi^f_{00}(\pm k\cos\theta_0)}{\alpha \mp k\cos\theta_0} \tag{36}$$

$$\xi^f_{0n}(\alpha) = \frac{e^{i(2ka - 3\pi/4)} i^n}{\pi(2a)^{n-1/2}} \Gamma^f_1[1/2 + n, -2i(\alpha + k)a] \tag{37}$$

$$\Gamma^f_m(u, v) = \int_0^\infty F_+[k + it/(2a)](t + v)^{-m} t^{u-1} e^{-t} dt \tag{38}$$

In (34), the unknowns $f^{us,ud}_n$ are determined by solving the appropriate matrix equations. The special function defined by (38) is the generalized gamma function introduced by the authors [8, 10] and rigorously accounts for the multiple-edge diffraction.

Thus, (34) provides high-frequency asymptotic solutions of the Wiener–Hopf equation, (19), and is valid for the waveguide slit width $2a$ being comparable to the incident wavelength or larger. Another Wiener–Hopf equation given by (20) can be solved in the same manner as mentioned previously, resulting in similar asymptotic solutions; hence, the details are omitted.

4. Scattered Field

The inverse Fourier transform of the scattered field is defined as follows:

$$\begin{aligned} \phi(x, z) = (2\pi)^{-1/2} \int_{-\infty+ic}^{\infty+ic} \Phi(x, \alpha) e^{-i\alpha z} d\alpha, \\ -k_2 < c < k_2 \cos\theta_0 \end{aligned} \tag{39}$$

First, we consider the region $|x| > b$ and derive the scattered far-field expression. We can easily show from (10), (19), and (20) that the scattered field for this region is expresses as

$$\Phi(x, \alpha) = \tilde{\Phi}(\alpha) e^{\mp\gamma x} \tag{40}$$

for $x \gtrless \pm b$, where

$$\begin{aligned} \tilde{\Phi}(\alpha) = &-\cosh(\gamma b)\left[e^{i\alpha a} U_{(+)}(\alpha) + e^{-i\alpha a} U_-(\alpha)\right]/(2\gamma) \\ &\mp \sinh(\gamma b)\left[e^{i\alpha a} V_{(+)}(\alpha) + e^{-i\alpha a} V_-(\alpha)\right]/(2\gamma), \quad x \gtrless \pm b \end{aligned} \tag{41}$$

In (41), $U_{(+)}(\alpha)$, $U_-(\alpha)$ and $V_{(+)}(\alpha)$, $V_-(\alpha)$ are the solutions to the Wiener–Hopf equations (19) and (20), respectively. Introducing the cylindrical coordinates $x = \rho\sin\theta$, $z = \rho\cos\theta$ $(-\pi < \theta < \pi)$ and applying the saddle point method, the scattered far field is derived as

$$\phi(\rho, \theta) \sim \tilde{\Phi}(-k\cos\theta) k \sin|\theta| e^{i(k\rho - \pi/4)}/(k\rho)^{1/2} \tag{42}$$

for $k\rho \to \infty$.

Next, we consider the region $|x| < b$ and derive the scattered field inside the waveguides. For this region, we

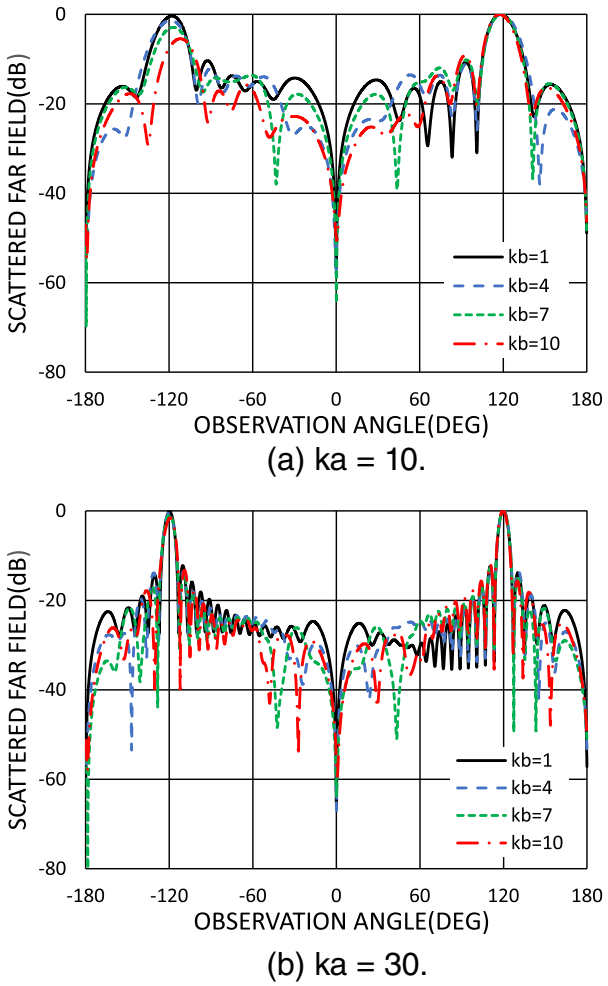

Figure 2. Normalized far-field intensity for E polarization $\theta_0 = 60°$.

substitute the field expression for $|x| < b$ in (10) into (39) and take into account the solutions of the Wiener–Hopf equations. By computing the residues at an infinite number of simple poles of the integrands, we obtain that

$$\phi(x,z) = \mp \sum_{n=1}^{\infty} \left[e^{\pm\gamma_n z}(-1)^n n\pi^{3/2}/\left(2^{3/2}b^2\gamma_n\right)\right] \cdot \{\Phi_1(b, \pm i\gamma_n)\sin[n\pi(x+b)/(2b)] - \Phi_1(-b, \pm i\gamma_n)\sin[n\pi(x-b)/(2b)]\}, \quad z \lessgtr \mp a \tag{43}$$

This completes derivation of the scattered field in real space.

5. Numerical Results and Discussion

We present numerical results on the far-field intensity and discuss scattering characteristics of the waveguide slit. For convenience, we define the normalized far-field intensity as

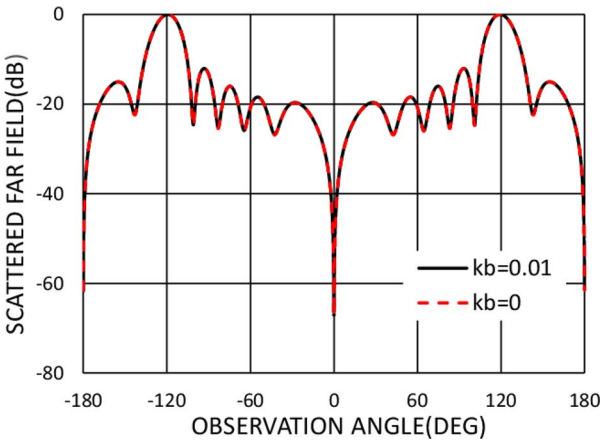

Figure 3. Normalized far-field intensity for E polarization $\theta_0 = 60°$, $ka = 10$, $kb = 0.01$ and its comparison with $kb = 0$ (slit in an infinite plane).

$$|\phi(\rho,\theta)|[\text{dB}] = 20\log_{10}\left[\frac{\lim_{\rho\to\infty}\left|(k\rho)^{1/2}\phi(\rho,\theta)\right|}{\max_{|\theta|\le\pi}\lim_{\rho\to\infty}\left|(k\rho)^{1/2}\phi(\rho,\theta)\right|}\right] \tag{44}$$

In numerical computation, we have chosen the same parameters as in the H-polarized case [6].

Figure 2 shows the normalized far-field intensity as a function of observation angle θ, where the slit width and the waveguide spacing are chosen as $ka = 10$, 30 and $kb = 1$, 4, 7, 10, respectively, and the incidence angle has been fixed as $\theta_0 = 60°$. Basic features observed for E polarization in this figure are similar to those for H polarization. In particular, for all chosen values of ka and kb, the far-field intensity shows noticeable peaks along the reflection boundary at $\theta = 120°$, as expected. We also see that for negative θ, the peak location gradually shifts from the incident shadow boundary at $-120°$, with an increase of kb. Figure 3 shows comparison of the results for $kb = 0.01$ and $kb = 0$ (a slit in an infinite, perfectly conducting plane [11, 12]) for E polarization $ka = 10$, $\theta_0 = 60°$. We observe that the two curves become very close to each other, as expected.

Finally, we compare the characteristics between H and E polarizations. Figure 4 shows the far-field intensity for $\theta_0 = 60°$, $ka = 30$, $kb = 1$, where the solid (black) and dashed (red) curves denote E and H polarizations, respectively. From the figure, we note that the intensity for positive θ shows close features for both polarizations except around $\theta = 0°$, $180°$. For negative θ, however, there are some differences between E and H polarizations. In particular, the intensity for both polarizations shows close features in the neighborhood of the incident direction, but except the main lobe

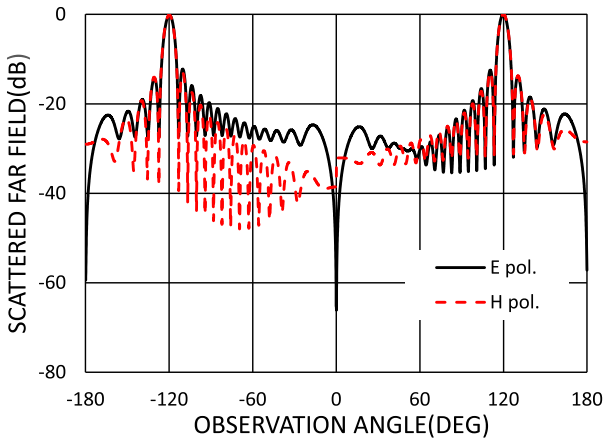

Figure 4. Comparison of the far-field intensity between two different polarizations for $\theta_0 = 60°$, $ka = 30$, $kb = 1$.

direction, differences are clearly seen between two polarizations.

6. Conclusion

In this two-part article, we have rigorously analyzed the plane-wave diffraction by a slit formed by two semi-infinite parallel-plate waveguides for both H polarization (Part I [6]) and E polarization (Part II, this article) using the Wiener−Hopf technique. The geometry considered here is of the modified Wiener−Hopf geometry of the first kind; hence, we have applied the method of solution developed in our previous article [7] to obtain a high-frequency asymptotic solution for this waveguide slit problem. Note that the geometry considered in this article belongs to a class of classical problems, but the final results obtained here are totally new. In particular, the high-frequency solutions obtained here rigorously consider the multiple-edge diffraction effects; hence, the results are even valid for the slit width comparable to the incident wavelength.

7. References

1. L. R. Alldredge, "Diffraction of Microwaves by Tandem Slits," *IRE Transactions on Antennas and Propagation*, **4**, 4, October 1956, pp. 640-649.
2. H. Levine and J. Schwinger, "On the Theory of Electromagnetic Wave Diffraction by an Aperture in an Infinite Plane Conducting Screen," *Communications on Pure and Applied Mathematics*, **3**, 4, December 1950, pp. 355-391.
3. S. C. Kashyap and M. A. K. Hamid, "Diffraction Characteristics of a Slit in a Thick Conducting Screen," *IEEE Transactions on Antennas and Propagation*, **19**, 4, July 1971, pp. 499-507.
4. B. Polat, A. Buyukaksoy, and G. Cinar, "Plane Wave Diffraction by Tandem Impedance Slits," *Progress in Electromagnetics Research*, **34**, January 2001, pp. 29-61.
5. S. Seran, J. P. Donohoe, and E. Topsakal, "Diffraction From a Material Loaded Tandem Slit," *IEEE Transactions on Antennas and Propagation*, **57**, 11, November 2009, pp. 3500−3511.
6. T. Nagasaka, W. Takahara, and K. Kobayashi, "Plane-Wave Diffraction by a Slit Formed by Two Semi-Infinite Parallel-Plate Waveguides—Part I: The Case of *H* Polarization," *Radio Science Letters*, **4**, 2022, pp. 1-5, doi: 10.46620/22-0055.
7. K. Kobayashi, "Solutions of Wave Scattering Problems for a Class of the Modified Wiener-Hopf Geometries," *IEEJ Transactions on Fundamentals and Materials*, **133**, 5, May 2013, pp. 233-241.
8. T. Nagasaka and K. Kobayashi, "Wiener-Hopf Analysis of the Plane Wave Diffraction by a Thin Material Strip," *IEICE Transactions on Electronics*, **E100-C**, 1, January 2017, pp. 11-19.
9. K. Kobayashi, "Wiener-Hopf and Modified Residue Calculus Techniques," in E. Yamashita (ed.), *Analysis Methods for Electromagnetic Wave Problems*, Boston, Artech House, 1990, Chapter 8.
10. K. Kobayashi, "On Generalized Gamma Functions Occurring in Diffraction Theory," *Journal of the Physical Society of Japan*, **60**, May 1991, pp. 1501-1512.
11. S. R. Seshadri, "High-Frequency Diffraction of Plane Waves by an Infinite Slit I & II," *Proceedings of the Indian National Science Academy*, **25**, 6A, November 1959, pp. 301-336.
12. S. Koshikawa, K. Kobayashi, and T. Eizawa, "Wiener-Hopf Analysis of the High-Frequency Diffraction by a Strip: Higher Order Asymptotics," *IEEJ Transactions on Fundamentals and Materials*, **113**, March 1993, pp. 157-166.